Mechatronics, Vol. 50, April 2018, pp. 422-433
DOI:10.1016/j.mechatronics.2017.02.001

Dual-Envelop-Oriented Moving Horizon Path Tracking Control for Fully Automated Vehicles

Hongyan Guo[a,b], Jun Liu[a,b], Dongpu Cao[c], Hong Chen[a,b,*], Ru Yu[b], Chen Lv[c]

[a]*State Key Laboratory of Automotive Simulation and Control, Jilin University, PR China*
[b]*Department of Control Science and Engineering, Jilin University, PR China*
[c]*Department of Automotive Engineer, Cranfield University, UK*

Abstract

A novel description of dual-envelop-oriented path tracking issue is presented for fully automated vehicles which considers shape of vehicle as inner-envelop (I-ENV) and feasible road region as outer-envelop (O-ENV). Then implicit linear model predictive control (MPC) approach is proposed to design moving horizon path tracking controller in order to solve the situations that may cause collision and run out of road in traditional path tracking method. The proposed MPC controller employed varied sample time and varied prediction horizon and could deal with modelling error effectively. In order to specify the effectiveness of the proposed dual-envelop-oriented moving horizon path tracking method, veDYNA-Simulink joint simulations in different running conditions are carried out. The results illustrate that the proposed path tracking scheme performs well in tracking the desired path, and could increase path tracking precision effectively.

Keywords: Fully automated vehicles, Path tracking, Model predictive control, Outer-envelop, Inner-envelop.

1. INTRODUCTION

With the rapid development of intelligent transportation systems [1] and automobile [2] technology, fully automated vehicles have arouse many researchers' attention due to various potential applications, for example reducing traffic congestion and traffic accidents, etc [3, 4, 5]. Fully automated vehicles are comprehensive applications of multi-discipline knowledge and theories, in

*Corresponding author. Tel(Fax): +86-431-85691900. Email: chenh@jlu.edu.cn

Published by Elsevier. This is the Author Accepted Manuscript issued with: Creative Commons Attribution Non-Commercial No Derivatives License (CC:BY:NC:ND 4.0).
The final published version (version of record) is available online at DOI:10.1016/j.mechatronics.2017.02.001. Please refer to any applicable publisher terms of use.

which perception, decision and control are the three main components of the software configuration [6]. In the aspect of control, one of the most important issues of fully automated vehicles is the path tracking problem [7, 8]. In general, path tracking for fully automated vehicles could be accomplished by steering control and velocity control [9, 10] according to the information of current vehicle dynamic states and the road in front of vehicle[11]. Steering control not only calculates and manipulates steering wheel to guide vehicles along the lateral path, but also related to lateral stability of vehicle. Therefore, it is a hot discussion for researchers [12].

The mainly discussed path tracking scheme is pure-pursuit tracking method [13], which considers vehicle as a rigid point with mass and it should track the desired path obtained by different methods [14]. Under this framework, a fuzzy logic controller for the path tracking of a wheeled mobile is presented in [15]. The controller is highly robust and flexible and it follows a sequence of discrete way-points, automatically. In [16], a robust H_∞ output-feedback control strategy for the path tracking of fully automated vehicles is presented. Besides, external disturbances of fully automated vehicles are considered here. For four-wheel independently actuated autonomous ground vehicles, a output constraint strategy using hyperbolic projection method and a integral sliding model-based composite nonlinear feedback control technique are presented in [17, 18, 19], respectively to deal with the lateral offset. The methods mentioned above could track the desired path of fully automated vehicles effectively. However, most of these control schemes are developed based on one-dimension vehicle-road model. It regards vehicle as a rigid point and uses a continuous curve or discrete points to describe the desired path. Compared with practical vehicle running situations, it may cause collisions when tracking a more complex road ignoring the size and shape of fully automated vehicles. Moreover, it is easy to run out of the feasible road region due to neglecting of the width of the path when using centerline to describe the desired path.

With the rapid development of online optimization [20] and hardware implementation [21], model predictive control (MPC) has attracted many focus on discussing vehicle active safety [22, 23, 24, 25] and path tracking issue of fully automated vehicles [7, 26, 27]. In [28], a nonlinear MPC method is presented to discuss path tracking control for autonomous vehicle system. In [6], it introduces an alternative MPC-based control framework that integrates local path planning with path tracking, in which the nominal path is commonly described in terms of curvature and arc

length. In [8], a collision avoidance system for an autonomous vehicle is presented, which consists of a motion planner and MPC-based active vehicle steering and active wheel torque control. MPC is able to systematically handle the constraints on state and control, and predict the dynamics of vehicle system, while generating an optimal sequence of control actions within a finite horizon based on the optimization technique. Accordingly, it is hot discussed and employed in vehicle path tracking issues. Therefore, the proposed methods above could track the desired path. However, the modelling error is not considered in the MPC approaches mentioned above which may affect control accuracy [29]. In addition, the path to be tracked is determined first, and could not changed. Moreover, the width of the vehicle is not considered, too. In order to solve those issues mentioned above, modelling error should be taken into consideration of the presented MPC method. The size and shape of vehicle, the width of the desired path should be considered. Moreover, the path to be tracked should be decided according the road information previewed ahead. The issues are preliminary discussed in [30], in which the description of path tracking for fully automated vehicles is carried out, and constraints that are used to restrict the vehicle position is considered. However, the influence of modelling error to path tracking precision has not been discussed. Besides, the path tracking controller is designed without considering different previewed road information.

In order to further discuss path tracking issue mentioned above, extended the path tracking scheme in [30], dual-envelop-oriented path tracking issue for fully automated vehicles is originally described in this manuscript. It takes the shape of vehicle as inner-envelop (I-ENV) and the feasible road region that considers the road width as outer-envelop (O-ENV). Then, a moving horizon path tracking controller employing implicit linear MPC method is designed considering the road boundaries, and actuator saturation as constraints. In order to obtain better control accuracy, the proposed MPC-based moving horizon path tracking scheme is considered the following aspects: the modelling error is discussed in the vehicle model, and the sample time and predictive horizon are varied according to road curvature. Finally, veDYNA-Simulink joint simulations are carried out to specify the effectiveness of the proposed moving horizon path tracking method.

The main contributions of this paper lie in two aspects: (1) The original description of dual-envelop-oriented path tracking issue of fully automated vehicle is presented which considers the shape of vehicle as inner-envelop and feasible road region as outer-envelop. (2) The moving hori-

zon path tracking controller that adopts varied sample time and varied prediction step is proposed, which could deal with the modelling error and increase path tracking precision effectively.

The remainder of the paper is organized as follows. Section 2 presents the dual-envelop-oriented path tracking problem. In Section 3, vehicle model is built and MPC-based moving horizon path tracking controller is designed. Simulations are carried out in Section 4. Brief conclusions of this paper are presented in Section 5.

2. Dual-envelop-oriented path tracking issue for fully automated vehicles

2.1. Dual-envelop-oriented path tracking issue

Considering the width and length of vehicle and the feasible road region in path tracking problem, a dual-envelop-oriented path tracking issue is shown in Fig. 1. The O-ENV that describes the feasible road region is represented by three curves: the centerline $f(x)$, the left boundary $f_l(x)$ and the right boundary $f_r(x)$. The left and right boundaries could be obtained by onboard camera. The I-ENV that represents the vehicle running in the feasible region is described as a rectangle, in which the width of vehicle is expressed as w and the length is described as l. Then the dual-envelop-oriented path tracking problem of fully automated vehicles could be split into two parts: searching the optimal path and tracking the optimal path.

When searching and tracking the optimal path in the dual-envelop-oriented region, it is essential to avoid crashing the road boundary in order to ensure the safety of fully automated vehicles. Based on the relationship between I-ENV and O-ENV, the aim could be achieved by restricting the lateral positions of the vehicle front end F and the rear end R within the O-ENV, that is

$$f_l(x) \leq y_i \leq f_r(r), i = F, R. \tag{1}$$

In addition, in order to simplified the path tracking problem, the I-ENV is shrink as a rigid bar. Accordingly each boundary of O-ENV is subtracted by a half width of vehicle to ensure the rationality of the simplification. Therefore, the simplified O-ENV could be described as

$$\begin{aligned} f_l^{'}(x) &= f_l(x) - \frac{w}{2}, \\ f_r^{'}(x) &= f_r(x) + \frac{w}{2}. \end{aligned} \tag{2}$$

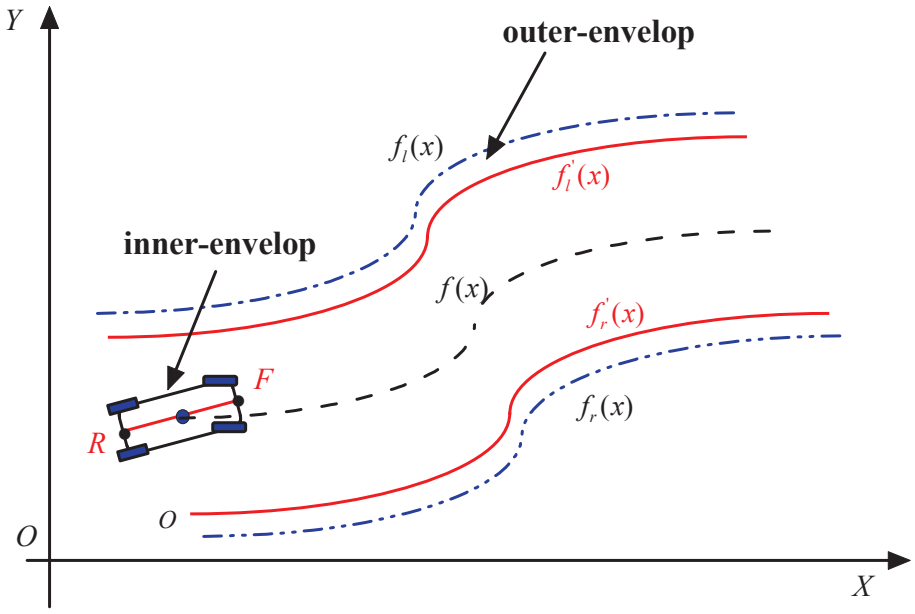

Figure 1: Dual-envelop for fully automated vehicles

Then the lateral positions of front and rear end of vehicle should satisfy the following conditions

$$f_r'(x) \leq y_i \leq f_l'(x), i = F, R. \tag{3}$$

where $y_i, i = F, R$ represents the lateral positions of the front end and rear end, respectively. Moreover, in order to keep vehicle running stably, it is better to make the vehicle follow the road centerline. It means that the difference between lateral vehicle position y and road centerline $f(x)$ should be as small as possible.

2.2. *Outer-envelop determination*

Considering the road information obtained from onboard sensors in the inertial coordinate system and the controller design based on the center of gravity (CoG) coordinate system, the transformation is carried out

$$\begin{bmatrix} x_r(i) \\ y_r(i) \\ x_l(i) \\ y_l(i) \end{bmatrix} = \begin{bmatrix} \cos\psi & \sin\psi & 0 & 0 \\ -\sin\psi & \cos\psi & 0 & 0 \\ 0 & 0 & \cos\psi & \sin\psi \\ 0 & 0 & -\sin\psi & \cos\psi \end{bmatrix} \cdot \begin{bmatrix} X_r(i) \\ Y_r(i) \\ X_l(i) \\ Y_l(i) \end{bmatrix} - \begin{bmatrix} X_{ro} \\ Y_{ro} \\ X_{lo} \\ Y_{lo} \end{bmatrix}. \tag{4}$$

Where $X_r(i), Y_r(i), X_l(i), Y_l(i)$ are the preview points of O-ENV in the inertial system, X_{ro}, Y_{ro}, X_{lo} and Y_{lo} are the initial points of O-ENV in the inertial system, $x_r(i), y_r(i), x_l(i)$ and $y_l(i)$ are the preview points in the vehicle coordinate system, respectively.

In order to describe the O-ENV, the cubic Lagrange interpolator is used to describe the two boundaries, in which the right boundary $f_r(x)$ and left boundary $f_l(x)$ could be written as:

$$f_r(x) = \sum \prod_{i \neq p} \frac{(x - x_r(i))}{(x_r(p) - x_r(i))} y_r(p), \quad p, i = j, n, m, k \tag{5a}$$

$$f_l(x) = \sum \prod_{i \neq p} \frac{(x - x_l(i))}{(x_l(p) - x_l(i))} y_l(p). \tag{5b}$$

Where, j, k, n and m represent four road data points in the given previewed points, which are selected through the quadratic search algorithm shown in Fig. 2.

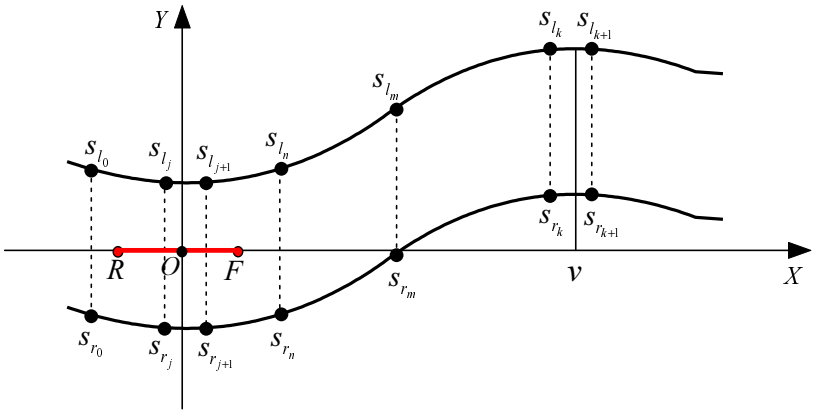

Figure 2: Schematic diagram of quadratic search

In order to find the nearest point of each boundaries in the horizontal direction behind of CoG that described as x_o, y_o, x_{r_0} and x_{l_0} are chosen as separated start points that are obtained from the last searching process. Since the negative vehicle speed did not consider in this paper, the horizontal displacement from x_r to x_o or from x_l and x_o must be negative, in which x_r and x_l are the point of right boundary and left boundary behind *CoG*. Therefore, it only needs to search points that the horizontal displacement satisfy the following equation

$$(x_r(j) - x_o) \cdot (x_r(j+1) - x_o) \leq 0, \tag{6a}$$

$$(x_l(j) - x_o) \cdot (x_l(j+1) - x_o) \leq 0. \tag{6b}$$

Where, $x_r(j)$ and $x_l(j)$ are the horizontal displacement of S_{r_j} and S_{l_j}, separately, $x_r(j+1)$ and $x_l(j+1)$ are the horizontal displacement of $S_{r_{j+1}}$ and $S_{l_{j+1}}$ shown in Fig. 2 respectively, and (S_{r_j}, S_{l_j}) is a set of points that is the nearest and behind CoG of vehicle.

The searching process will continue in order to obtain the closest point to the preview point. It consumes the determined points in Eq. (6) as start point should satisfies the following equations

$$(x_r(k) - v \cdot T) \cdot (x_r(k+1) - v \cdot T) \leq 0, \tag{7a}$$

$$(x_l(k) - v \cdot T) \cdot (x_l(k+1) - v \cdot T) \leq 0. \tag{7b}$$

Where the length of the O-ENV is selected as $v \cdot T$. Besides $T = 1$ and v is longitudinal velocity of CoG. In addition, $x_r(k)$ and $x_l(k)$ are the horizontal displacement of S_{r_k} and S_{l_k}, respectively, $x_r(k+1)$ and $x_l(k+1)$ are the horizontal displacement of $S_{r_{k+1}}$ and $S_{l_{k+1}}$, separately, and $(S_{r_{k+1}}, S_{l_{k+1}})$ is a set of the nearest point to (S_{r_k}, S_{l_k}). When the above equations are satisfied, it is specified that the closest point to the preview point is (S_{r_k}, S_{l_k}).

The two sets of points (S_{r_j}, S_{l_j}) and (S_{r_k}, S_{l_k}) are regarded as the first and final interpolation points, respectively. The positions of the four road data points are expressed as j, k, n and m, then the other two interpolation point can be calculated as

$$n = \left\lfloor \frac{k-j}{3} + j \right\rfloor, \tag{8a}$$

$$m = \left\lfloor \frac{k-j}{3} + n \right\rfloor. \tag{8b}$$

Where n represents the position of (S_{r_n}, S_{l_n}), and m represents the position of (S_{r_m}, S_{l_m}).

When the O-ENV is determined, the road centerline could also be expressed as follows

$$f(x) = \frac{1}{2}\left(f_l(x) + f_r(x)\right). \tag{9}$$

3. Moving horizon path tracking controller design

In this section, vehicle model is described, and then the moving horizon path tracking controller with varied sample time and varied predictive horizon is presented.

3.1. Vehicle model

Assuming vehicle as a rigid body with non-deformable wheels, the kinematic of vehicle could be obtained according to the geometry relationship described in Fig. 3 (a),

$$\dot{x}_o = v\cos(\psi+\beta), \tag{10a}$$

$$\dot{y}_o = v\sin(\psi+\beta), \tag{10b}$$

$$\dot{\psi} = r, \tag{10c}$$

where x_o and y_o are the longitudinal and lateral positions of CoG, r is the yaw rate, β is the

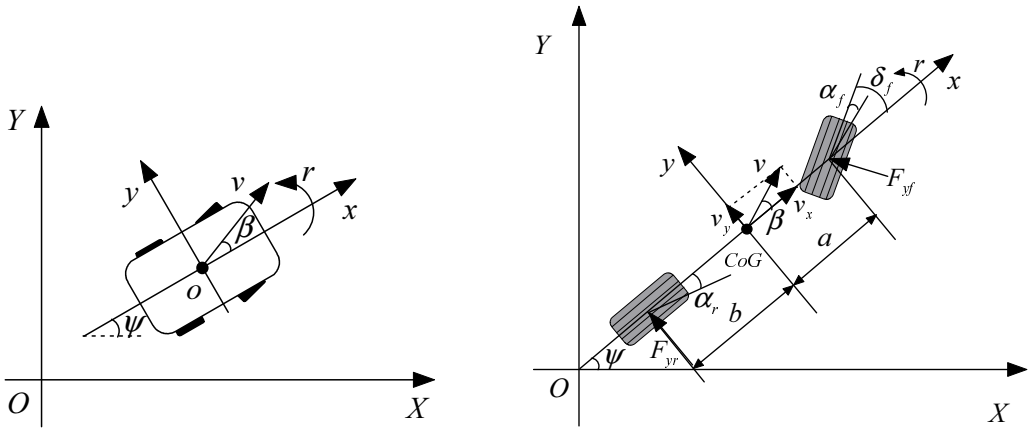

(a) Vehicle kinematic relation (b) 2-DOF vehicle model

Figure 3: Vehicle model

vehicle sideslip angle, ψ is the yaw angle, and v is longitudinal velocity of CoG. Considering the observable distance of fully automated vehicles in a sample time is about 50 meters and the curvature of road is small, it leads to small variances of vehicle sideslip angle and yaw angle. Therefore, it assumes $\sin(\psi+\beta)\approx\psi+\beta$, $\cos(\psi+\beta)\approx 1$ reasonably. Accordingly, the model could be described as

$$\dot{x}_o = v, \tag{11a}$$

$$\dot{y}_o = v(\psi+\beta), \tag{11b}$$

$$\dot{\psi} = r. \tag{11c}$$

Moreover, regarding the vehicle dynamics that is shown in Fig. 3 (b), the vehicle body coordinate system with the origin at CoG is defined. The direction of longitudinal velocity points to forward and the lateral velocity points to the left, the directions of vertical velocity, and other forces and torques are ascertained by the righthand rule. Assuming the longitudinal velocity is constant, the lateral dynamics of vehicle according to the Newton's Law could be derived as follows

$$\begin{aligned} mv(\dot{\beta}+r) &= F_{xf}\sin\delta_f + F_{yf}\cos\delta_f + F_{yr}, \\ I_z\dot{r} &= a(F_{xf}\sin\delta_f + F_{yf}\cos\delta_f) - bF_{yr}, \end{aligned} \tag{12}$$

where m is the vehicle mass, I_z is the moment of inertia of the vehicle around z-axis, a and b are the distances from the center of gravity to the front and rear axles, respectively, F_{yf} and F_{yr} are the front and rear lateral tire forces, respectively, and δ_f is the front wheel steering angle. The linear tire model is employed to describe the front and rear lateral tire forces

$$\begin{aligned} F_{yf} &= C_f\alpha_f, \\ F_{yr} &= C_r\alpha_r, \end{aligned} \tag{13}$$

where C_f, C_r are the cornering stiffness of tire, respectively. In addition, considering the front wheel steering angle is small when the vehicle runs stably, the approximation is carried out $\sin\delta_f \approx 0$, $\cos\delta_f \approx 1$. Therefore, the front and rear tire sideslip angles of vehicle α_f and α_r could be approximate as follows [29]

$$\begin{aligned} \alpha_f &= \beta + \frac{ar}{v} - \delta_f, \\ \alpha_r &= \beta - \frac{br}{v}. \end{aligned} \tag{14}$$

Then substituting Eq. (13) and Eq. (14) into Eq. (12), and combined with Eq. (11), the lateral dynamics of fully autonomous vehicle could be described as follows

$$\begin{aligned} \dot{y}_o &= v(\psi+\beta), \\ \dot{\psi} &= r, \\ \dot{\beta} &= \frac{(C_f+C_r)}{mv}\beta + (\frac{(aC_f-bC_r)}{mv^2} - 1)r - \frac{C_f}{mv}\delta_f, \\ \dot{r} &= \frac{(aC_f-bC_r)}{I_z}\beta + \frac{(a^2C_f+b^2C_r)}{I_zv}r - \frac{aC_f}{I_z}\delta_f. \end{aligned} \tag{15}$$

Selecting lateral position y_o as output, front wheel steering angle δ_f as input, and $x = [y_o \ \psi \ \beta \ r]$ as the states, then the system shown in Eq. (15) could be described as follows

$$\dot{x} = Ax + B\delta_f, \tag{16a}$$

$$y = Cx, \tag{16b}$$

where

$$\boldsymbol{A} = \begin{bmatrix} 0 & v & v & 0 \\ 0 & 0 & 0 & 1 \\ 0 & 0 & \frac{C_f+C_r}{mv} & \frac{aC_f-bC_r}{mv^2}-1 \\ 0 & 0 & \frac{aC_f-bC_r}{I_z} & \frac{a^2C_f+b^2C_r}{I_z v} \end{bmatrix}, \boldsymbol{B} = \begin{bmatrix} 0 \\ 0 \\ -\frac{C_f}{mv} \\ -\frac{aC_f}{I_z} \end{bmatrix}, \boldsymbol{C} = \begin{bmatrix} 1 \\ 0 \\ 0 \\ 0 \end{bmatrix}^{\mathrm{T}}.$$

Then, by discretizing Eq. (16) at sample time T_s with Euler method, the discrete-time model could consequently obtained as follows

$$\begin{aligned} x(k+1) &= A_c x(k) + B_c \delta_f(k), \\ y(k) &= C_c x(k), \end{aligned} \tag{17}$$

where $A_c = e^{AT_s}, B_c = \int_0^{T_s} e^{A\tau} d\tau \cdot B, C_c = C$ are the discrete matrices.

The assumptions mentioned above such as $\sin(\psi+\beta) \approx \psi+\beta$, $\sin\delta_f \approx 0$ in Eq. (15) could introduce modelling error that could be seen in Fig. 4, which causes the lateral position of vehicle deviating the actual value. In addition, additional disturbance could also introduce the error of lateral position of fully automated vehicles. It could be seen in Eq. (15) that the lateral position of vehicle is the function of longitudinal velocity of CoG, yaw angle ψ, and sideslip angle β. The simplification and the disturbance of yaw angle and sideslip angle brings the modelling error of vehicle lateral position. Therefore, the modelling error is additional considered in fully automated vehicles modelling as follows

$$\begin{aligned} x(k+1) &= A_c x(k) + B_c \delta_f(k) + B_{dc} d(k), \\ y(k) &= C_c x(k). \end{aligned} \tag{18}$$

Where $B_{c2} = [\ 0 \quad 0 \quad K_r \quad K_\beta\ ]^T$ is the modelling error matrix and its discrete form could be computed as $B_{dc} = \int_0^{T_s} e^{A\tau} d\tau \cdot B_{c2}$. Considering yaw rate could be measured directly, define $d = r_m - r$, where r is the state of fully automated vehicle and r_m is the measured yaw rate.

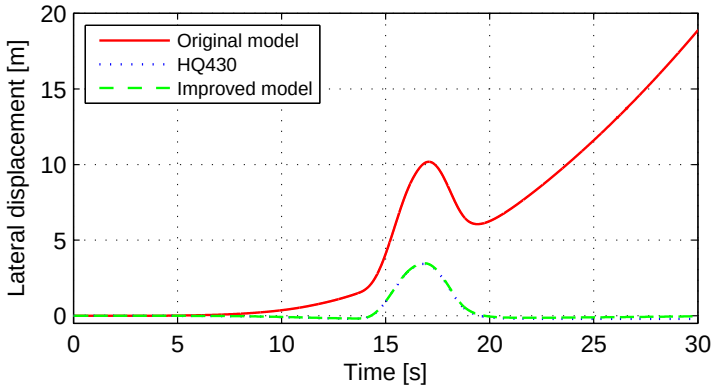

(a) lateral position of vehicle y_o

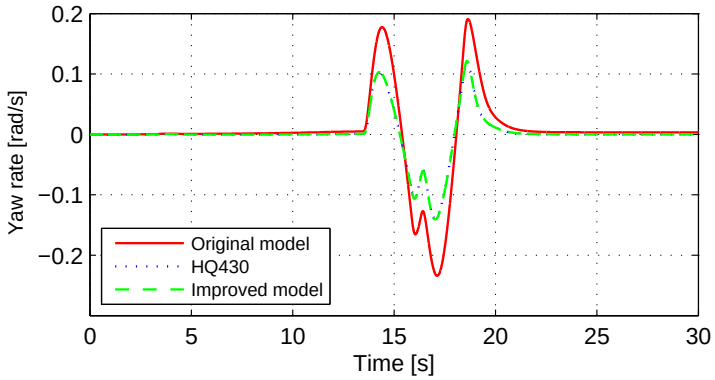

(b) yaw rate r

Figure 4: Validation for fully automated vehicle modelling

Remark 3.1. *The simplified cases such as* $\sin(\psi+\beta)\approx\psi+\beta$, $\cos(\psi+\beta)\approx 1$ *and* $\sin\beta\approx 0$ *are reasonable as mentioned above. In fact,* $\sin(\psi+\beta)\approx\psi+\beta$, $\cos(\psi+\beta)\approx 1$ *and* $\sin\beta\approx 0$ *could be adopted here, directly. Accordingly, the dual-envelop-oriented path tracking problem is a nonlinear optimization issue that need nonlinear MPC to solve. In this case, the computational time of optimization in nonlinear MPC will be much more than the linear MPC, which is not suitable for real vehicle application. In this manuscript, the dual-envelop-oriented moving horizon tracking control scheme is tested on fully automated vehicle similar with [31], which will be introduced in our next paper. Therefore, considering real vehicle application, the simplified cases mentioned above are chosen and the implicit linear MPC is adopted here.*

3.2. Path tracking controller design based on MPC

Considering the road and traffic are all varied instantaneously, it needs fully automated vehicle to make decision in each sample time correspondingly. In addition, the feasible region obtained from the above subsection restricts the vehicle lateral position, which is considered as constraints of system. Therefore, model predictive control approach is introduced to discuss moving horizon path tracking controller design.

3.2.1. prediction

The control scheme for dual-envelop-oriented path tracking issue of full automated vehicles is shown in Fig. 5. Due to the vehicle states estimation schemes have already been discussed extensively in [32, 33, 34], it is assumed that the vehicle velocity, yaw angle, sideslip angle and tire-road friction coefficient could be estimated directly. In addition, the control of actuator that is steering motor is not considered in this manuscript. The road information module in Fig. 5 is used to obtain the boundary information of O-ENV, which has been introduced in the above subsection. Suppose that the predictive step is P, the control step is N. According to the current

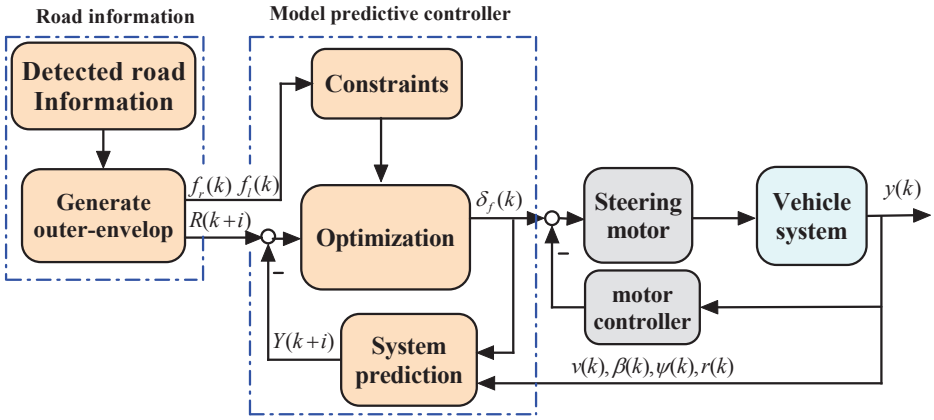

Figure 5: Block diagram of the path following control system

fully automated vehicle's state, the future vehicle states could be predicted as follows

$$\begin{aligned} x(k+1) &= A_c x(k) + B_c \delta_f(k) + B_{dc} d(k), \\ x(k+2) &= A_c^2 x(k) + A_c B_c \delta_f(k) + B_c \delta_f(k+1) + (A_c B_{dc} + B_{dc}) d(k), \\ &\vdots \end{aligned} \tag{19}$$

$$
\begin{aligned}
x(k+N) &= A_c^N x(k) + A_c^{N-1} B_c \delta_f(k) + \cdots + B_c \delta_f(k+N-1) + \sum_{i=1}^{N-1} A_c^i B_{dc} d(k), \\
&\vdots \\
x(k+P) &= A_c^P x(k) + A_c^{P-1} B_c \delta_f(k) + \cdots + \sum_{i=1}^{P-N+1} A_c^{i-1} B_c \delta_f(k+N-1) + \sum_{i=1}^{P-1} A_c^i B_{dc} d(k).
\end{aligned}
$$

When the sample time exceeds the control step N, it assumes that the control input keeps invariant, that is $u(k+N) = u(k+N+1) = \cdots = u(k+P-1)$. In this case, the output expression could be predicted as:

$$
\begin{aligned}
y(k+1) &= C_c A_c x(k) + C_c B_c \delta_f(k) + C_c B_{dc} d(k), \\
y(k+2) &= C_c A_c^2 x(k) + C_c A_c B_c \delta_f(k) + C_c B_c \delta_f(k+1) + (C_c A_c B_{dc} + C_c B_{dc}) d(k), \\
&\vdots \\
y(k+N) &= C_c A_c^N x(k) + C_c A_c^{N-1} B_c \delta_f(k) + \cdots + C_c B_c \delta_f(k+N-1) + \sum_{i=1}^{N-1} C_c A_c^i B_{dc} d(k), \\
&\vdots \\
y(k+P) &= C_c A_c^P x(k) + C_c A_c^{P-1} B_c \delta_f(k) + \cdots + \sum_{i=1}^{P-N+1} C_c A_c^{i-1} B_c \delta_f(k+N-1) + \sum_{i=1}^{P-1} C_c A_c^i B_{dc} d(k).
\end{aligned}
\tag{20}
$$

By defining the vectors and matrices as follows:

$$
S_x = \begin{bmatrix} C_c A_c \\ \vdots \\ C_c A_c^N \\ \vdots \\ C_c A_c^P \end{bmatrix}, \; S_{xu} = \begin{bmatrix} B_c & 0 & \cdots & 0 \\ \vdots & \vdots & \ddots & \vdots \\ A_c^{N-1} B_c & A_c^{N-2} B_c & \cdots & B_c \\ \vdots & \vdots & \ddots & \vdots \\ A_c^{P-1} B_c & A_c^{P-2} B_c & \cdots & \sum_{i=1}^{P-N+1} A_c^i B_c \end{bmatrix}, \quad S_{xd} = \begin{bmatrix} B_{dc} \\ A_c B_{dc} + B_{dc} \\ \vdots \\ \sum_{i=1}^{P-1} A_c^i B_{dc} \end{bmatrix},
$$

$$
S_u = \begin{bmatrix} C_c B_c & 0 & \cdots & 0 \\ \vdots & \vdots & \ddots & \vdots \\ C_c A_c^{N-1} B_c & C_c A_c^{N-2} B_c & \cdots & C_c B_c \\ \vdots & \vdots & \ddots & \vdots \\ C_c A_c^{P-1} B_c & C_c A_c^{P-2} B_c & \cdots & \sum_{i=1}^{P-N+1} C_c A_c^i B_c \end{bmatrix}, \; \delta_f(k) = \begin{bmatrix} \delta_f(k) \\ \delta_f(k+1) \\ \vdots \\ \delta_f(k+N-1) \end{bmatrix},
$$

$$\boldsymbol{Y}(k+1|k)=\begin{bmatrix} y_(k+1) \\ y_(k+2) \\ \vdots \\ y_(k+P) \end{bmatrix}, \boldsymbol{x}(k+1|k)=\begin{bmatrix} x_(k+1) \\ x_(k+2) \\ \vdots \\ x_(k+P) \end{bmatrix}, S_{xx}=\begin{bmatrix} A_c \\ \vdots \\ A_c^N \\ \vdots \\ A_c^P \end{bmatrix}, S_d=\begin{bmatrix} C_cB_{dc} \\ C_cA_cB_{dc}+C_cB_{dc} \\ \vdots \\ \sum_{i=1}^{P-1} C_cA_c^iB_{dc} \end{bmatrix}.$$

the N steps of the prediction state and output equation can be summarized as

$$\begin{aligned} X(k+1 \mid k) &\triangleq S_{xx}x(k)+S_{xu}\delta_f(k)+S_{xd}d(k), \\ Y(k+1 \mid k) &\triangleq S_x x(k)+S_u\delta_f(k)+S_d d(k). \end{aligned} \tag{21}$$

According to the analysis of the dual-envelop-oriented path tracking problem described in Section 2, one of the control requirement is making fully automated vehicles travel along the centerline of the road region as far as possible, thus the reference input sequence is defined as:

$$R(k)=\begin{bmatrix} f(k), & f(k+1), & \cdots, & f(k+P-1) \end{bmatrix}^T, \tag{22}$$

where $f(k+i-1)$ comes from the discretization of the centerline that is computed in Eq. (9).

3.2.2. optimization

Then in order to follow the centerline in the given feasible region, it requires to minimize the difference between the predicted output and road centerline, that is

$$J_1 = \| Y(k+1|k)-R(k) \|^2. \tag{23}$$

In addition, considering the saturation of mechanical system, the action of steering wheel motor is limited. Accordingly, the requirement is formulated as minimizing:

$$J_2 = \|U(k)\|^2, \tag{24}$$

Besides, it ensures that fully automated vehicles consume a low energy by minimizing driving route as follows

$$J_3 = \sum_{i=1}^{P}(\|\Delta x_d(k+i)\|^2+\|\Delta y_d(k+i)\|^2), \tag{25}$$

where $\Delta x_d(k+i)=v(k)\cdot T_s$, $\Delta y_d(k+i)=y_o(k+i)-y_o(k+i-1)$, $i=1,\cdots,P$ is longitudinal and lateral distances in a sample time, respectively.

Considering minimizing J_1, J_2 and J_3 simultaneously is contradictive, weighting factors are introduced. Accordingly, the multi-objective cost function could be obtained as follows:

$$J = \|\Gamma_y(Y(k+1|k) - R(k))\|^2 + \|\Gamma_u U(k)\|^2 + \sum_{i=1}^{P} \Gamma_{d,i}(\|\Delta x_d(k+i)\|^2 + \|\Delta y_d(k+i)\|^2), \tag{26}$$

where $\Gamma_y = \text{diag}(\Gamma_{y,1}, \Gamma_{y,2}, \cdots, \Gamma_{y,P}) > 0$, $\Gamma_u = \text{diag}(\Gamma_{u,1}, \Gamma_{u,2}, \cdots, \Gamma_{u,N}) > 0$ are the weighting matrices, $\Gamma_{d,i} > 0, i = 1, 2, \cdots p$ are the weighting factors.

According to the geometric relationships, the movement direction of the vehicle shown in Fig. 6 and small angle assumption [29], the relationship among vehicle lateral position y_o, front-end F and rear-end R could be described as

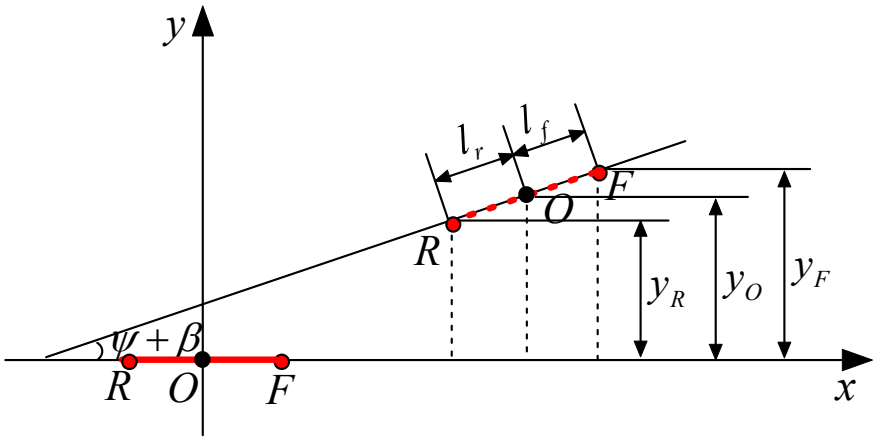

Figure 6: Geometric relationship between movement direction

$$\begin{aligned} y_F &= y_o + l_f(\psi + \beta), \\ y_R &= y_o - l_r(\psi + \beta). \end{aligned} \tag{27}$$

Substituting Eq. (27) into Eq. (3), then the output of the vehicle system is considered to satisfy the following constraints in discrete form

$$f_r'(k+i) - l_f(\psi + \beta) \le y(k+i) \le f_l'(k+i) - l_f(\psi + \beta), \tag{28a}$$

$$f_r'(k+i) + l_r(\psi + \beta) \le y(k+i) \le f_l'(k+i) + l_r(\psi + \beta), \tag{28b}$$

where $i = 1, \cdots, P$, $\psi(k+i) = [0\ 1\ 0\ 0]x(k+i)$, $f_l'(k+i)$ and $f_r'(k+i)$ are discrete forms of the left and right boundaries of the given O-ENV, respectively.

Moreover, considering the mechanical characteristic of steering actuator, it bounds the steering variation and steering rate. In order to ensure a practical control variable, the following constraints of control input and its variation are also considered as follows

$$\Delta\delta_{f_{min}} \leq \Delta\delta_f(k+i) \leq \Delta\delta_{f_{max}}, \tag{29a}$$

$$\delta_{f_{min}} \leq \delta_f(k+i) \leq \delta_{f_{max}}, \tag{29b}$$

where $\Delta\delta_f(k+i) = \delta_f(k+i+1) - \delta_f(k+i)$, $i = 0, \cdots, N-1$ is the control increment, δ_{fmax} is the maximum front steering wheel angle and δ_{fmin} is the minimum front steering wheel angle. The maximum and minimum front steering wheel angle could be computed from corresponding steering wheel angle, that is $\delta_{fmax} = \frac{\delta_{max}}{\rho}$ and $\delta_{fmin} = \frac{\delta_{min}}{\rho}$. Where ρ is the steering gear ratio, δ_{max} is the maximum steering wheel angle and δ_{min} is the minimum steering wheel angle. The maximum and minimum steering wheel angle is constant for a certain vehicle. In fact, the steering gear ratio is affected by longitudinal velocity mainly and also influenced by some other road parameters. Due to the longitudinal velocity is considered constant here, it consumed that the steering gear ratio is constant and accordingly the maximum and minimum front steering wheel angle is computed as constant here. For further research, the varied steering ratio will be considered in details. In conclusion, the dual-envelop-oriented moving horizon path tracking problem can be described by the following optimization problem

$$\begin{aligned}
\min_{U(k)} \quad & J = \|\Gamma_y(Y(k+1|k) - R(k))\|^2 + \|\Gamma_u U(k)\|^2 + \sum_{i=1}^{P} \Gamma_{d,i}(\|\Delta x_d(k+i)\|^2 + \|\Delta y_d(k+i)\|^2) \\
\textbf{s.t.} \quad & x(k+i+1) = A_c x(k+i) + B_c \delta_f(k+i) + B_{dc} d(k), \\
& y_o(k+i+1) = C_c x(k+i), \\
& f_r^{'}(k+i) - l_f(\psi+\beta) \leq y_o(k+i) \leq f_l^{'}(k+i) - l_f(\psi+\beta), \\
& f_r^{'}(k+i) + l_r(\psi+\beta) \leq y_o(k+i) \leq f_l^{'}(k+i) + l_r(\psi+\beta), \\
& \left|\delta_f(k+i)\right| \leq \delta_{fsat}, \\
& \left|\Delta\delta_f(k+i)\right| \leq \dot{\delta}_{fsat} * T_s.
\end{aligned} \tag{30}$$

After successfully solving the model predictive control problem where 'fmincon' in Matlab is employed considering future expansion research, the first element of the optimal control sequence

$U(k)$ is applied to the vehicle system. Then the predictive horizon is moved forward one interval, and the optimization problem is solved again by using new process measurements.

3.2.3. Discussion of parameters choosing

The chosen of sample time T_s and predictive horizon are discussed here because of sample time T_s related to the precision of discrete-time model and predictive horizon $t_p = P * T_s$ corresponding to control performance. Weighting matrices $\Gamma_y, \Gamma_u, \Gamma_{d,i}$ aims at solving the problem of the proportion of various control objectives in Eq. (23) - Eq. (25) which rely on the importance of different control objectives allocated by control system, therefore it is not been discussed here in detail.

choosing of sample time T_s: Different sample time is chosen from $[0.01\ 0.2]$ and double lane change manoeuvre is carried out, where the longitudinal velocity is $v = 70$ km/h and tire-road friction coefficient is $\mu = 0.9$. The simulation results are shown in Fig. 7. It could be seen in Fig. 7 (a) that the smaller sample time T_s and the smaller tracking error, the better control performance. However, the decrease of sample time, the amplitude of front steering angle is increased that is shown in Fig. 7 (b). Accordingly, the amplitudes of yaw rate, sideslip angle and lateral acceleration shown in Fig. 7 (c)-(e) are also increased. It specifies that the vehicle could track the desired road centerline when the lateral acceleration at about 5 m/s^2. However, the lateral stability of vehicle is deteriorated. Moreover, It could be concluded from Fig. 7 (f) that the computational time of MPC controller is increased with the decrease of sample time. Therefore, the chosen of sample time is a tradeoff between tracking performance, lateral stability and computational time. In addition, considering road curvature is a key factor for path tracking, a varied sample time strategy based on road curvature is adopted that is similar with [35] in the controller design

$$T_s = \text{round}(5 + 10 \cdot \text{e}^{-\omega \cdot \text{PGC}})/100, \tag{31}$$

where

$$PGC = \frac{1}{P-2} \sum_{i=0}^{P-2} \left| \frac{y_r(k+i+2) - 2y_r(k+i+1) + y_r(k+i)}{2\Delta x_d(k+i)} \right|$$

is the two order derivative average of the desired road, function of round$(\cdot)$ is round up and round down, ω is contraction factor.

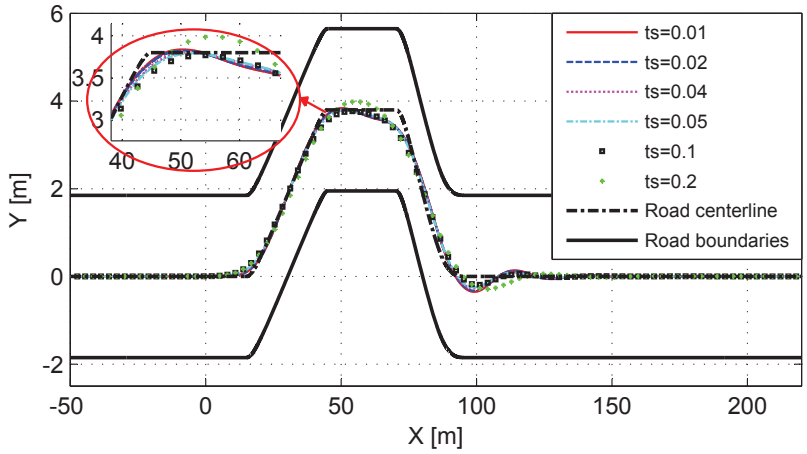

(a) vehicle trajectory

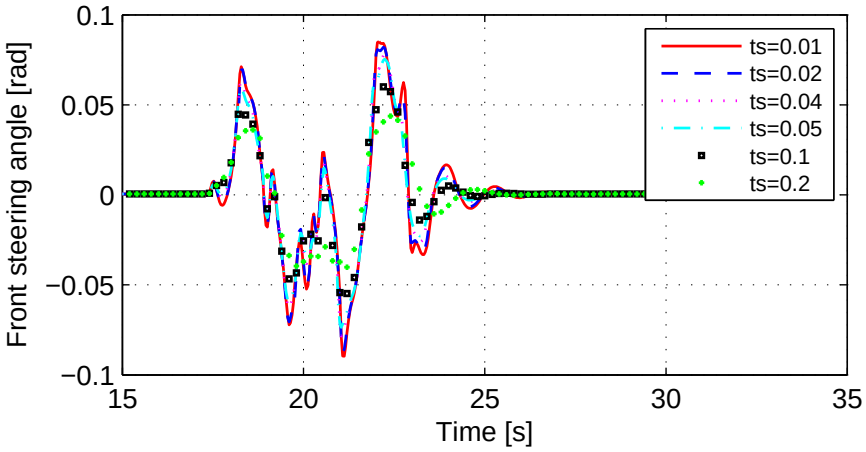

(b) optimized front steering angle δ_f

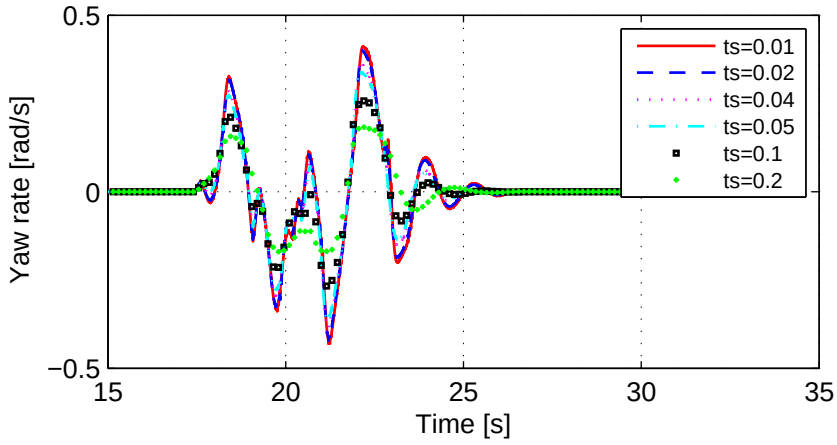

(c) yaw rate r

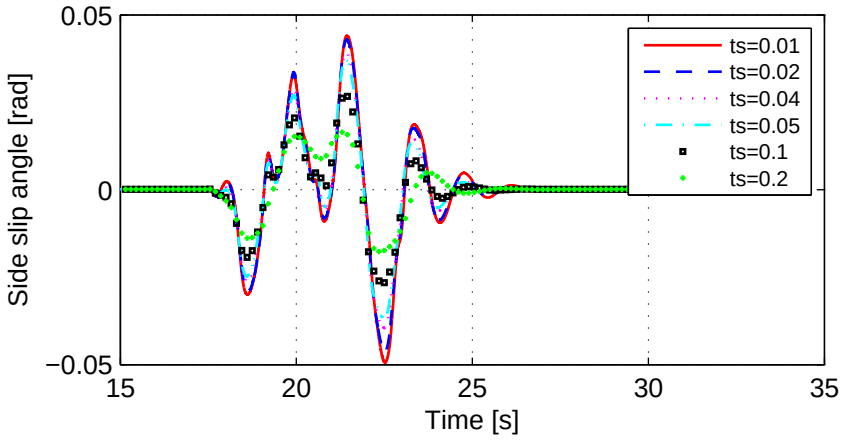

(d) sideslip angle β

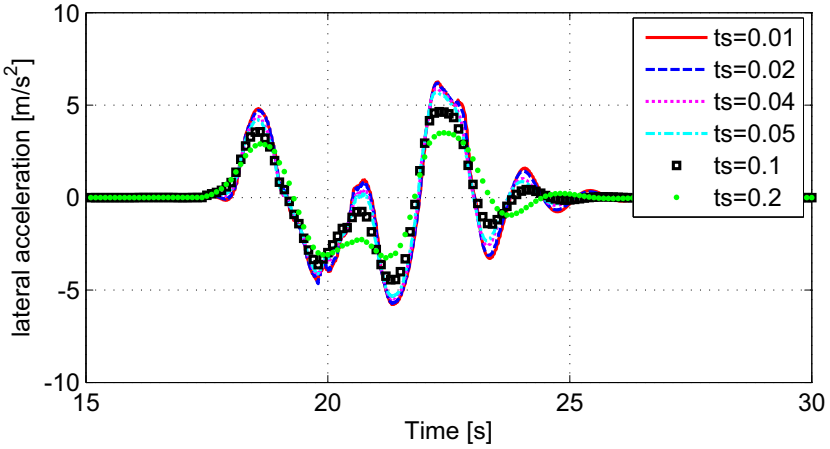

(e) lateral acceleration

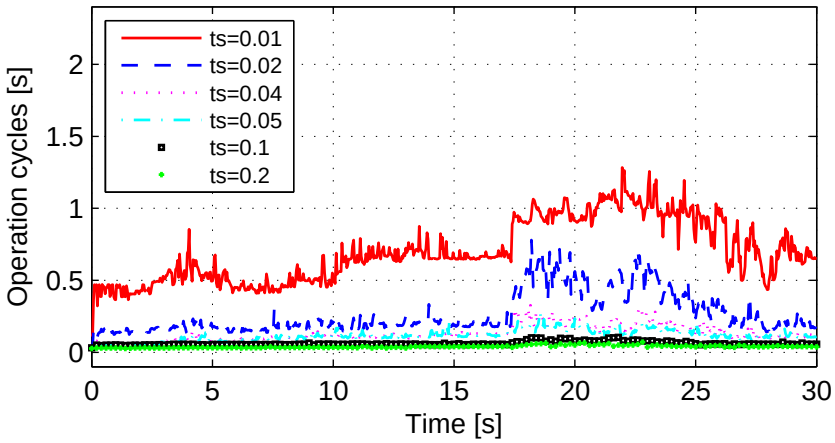

(f) computational time

Figure 7: Simulation results with different sample times

choosing of predictive horizon t_p: Considering the relationship among sample time, prediction step and predictive horizon $t_p = P \cdot T_s$, the predictive step is decided by sample time and predictive horizon. In order to specify the dual-envelop-oriented path tracking performance in different predictive horizon, the simulations of double lane change manoeuvre are carried out, where the sample time $T_s = 0.01$, and predictive horizon is varied in the range between $t_p \in [0.5\ 1.5]$. Accordingly, the simulation results are shown in Fig. 8, clearly. It could be seen from Fig. 8 (a) that the tracking error is relatively bigger than others when the predictive horizon is smaller than 1s. It is even unstable when the predictive horizon is smaller than 0.8s that could be concluded from Fig. 8 (b) and (c). Therefore, it could be concluded that the smaller predictive horizon will be, the

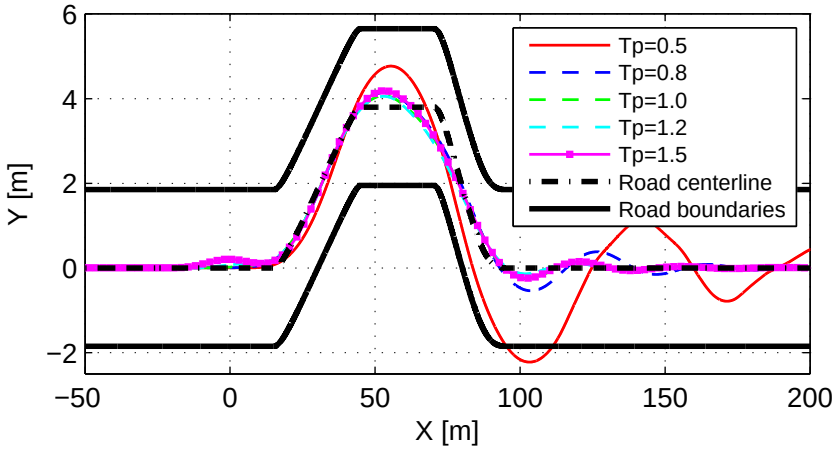

(a) vehicle trajectory

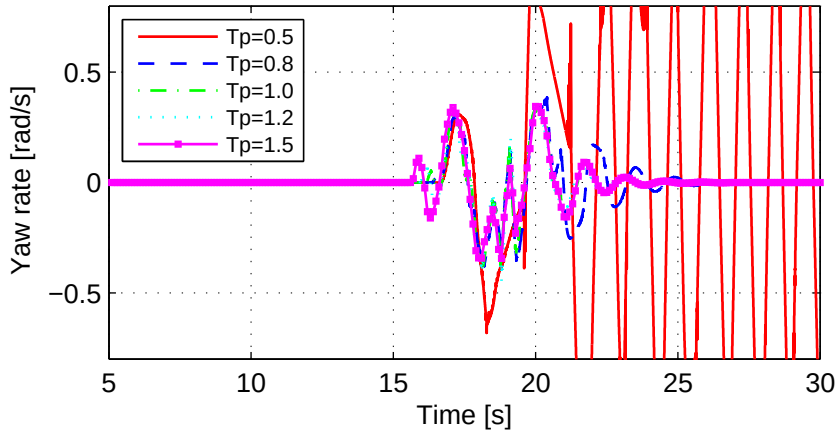

(b) yaw rate r

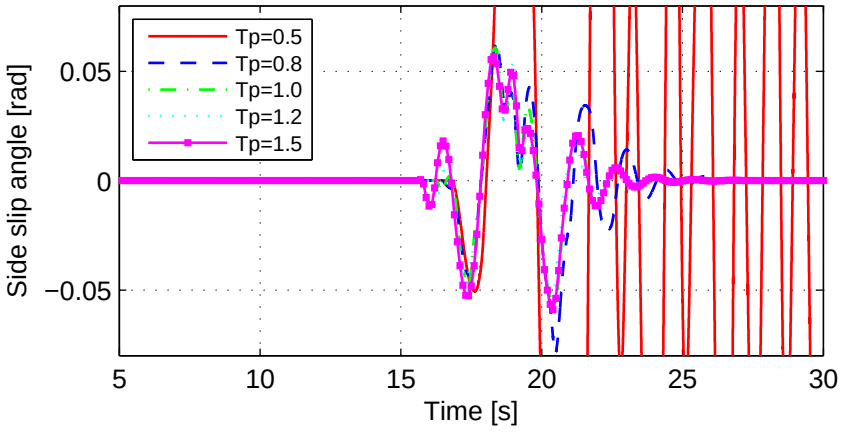

(c) sideslip angle β

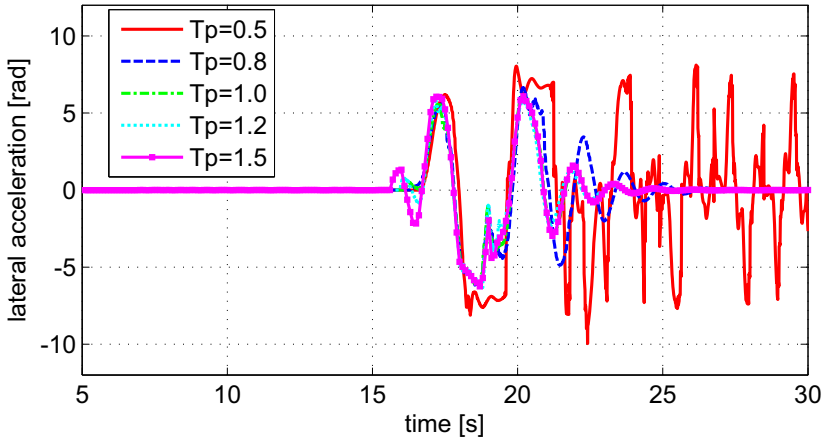

(d) lateral acceleration a_y

Figure 8: Simulation results with different predictive horizons

larger tracking error could be obtained. Accordingly, the vehicle could not keep stable in this situation. Moreover, it can be seen from Fig. 8 (d) that the lateral acceleration could be achieve more that 5 m/s^2 when the predictive horizon is larger than 0.8s. In addition, the premature vehicle turning could happen when the predictive horizon is larger than 1.2s seen from Fig. 8 (a), clearly. Therefore, the predictive horizon ranges from 0.8 to 1.1, that is $t_p \in [0.8\ 1.1]$. Furthermore, according to the predictive characteristic of human driver, the varied predictive horizon is adopted as follows

$$t_p = \text{round}(80 + 30 \cdot \text{e}^{-\omega \cdot \text{PGC}})/100. \tag{32}$$

It could be concluded from Eq. (31) and Eq. (32) that the variance of predictive horizon keeps consistent with sample time, which are reduced by the increasing of road curvature. It will relieve the situation that the computational cost is increased with the sample time decreased. Therefore, the varied sample time and predictive horizon release the computational burden, effectively.

4. Simulations

In order to verify the effectiveness of the proposed dual-envelop-oriented moving horizon path tracking method, high-fidelity software veDYNA® is employed here. veDYNA® is a proven and versatile vehicle dynamics simulation tool, which the open and modular model architecture implemented in MATLAB and Simulink allows easy and straightforward incorporation of user-specific

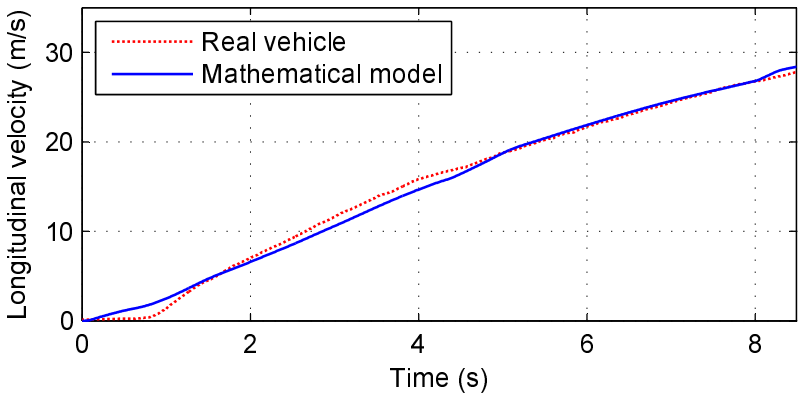

(a) longitudinal vehicle velocity

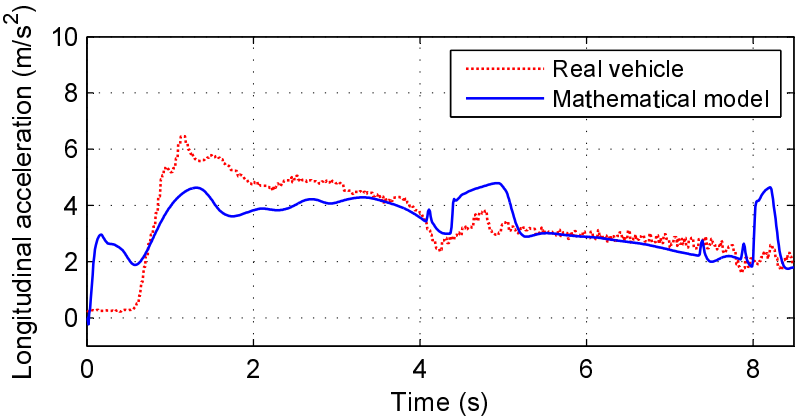

(b) longitudinal acceleration

Figure 9: Results comparison of one hundred kilometers acceleration experiment

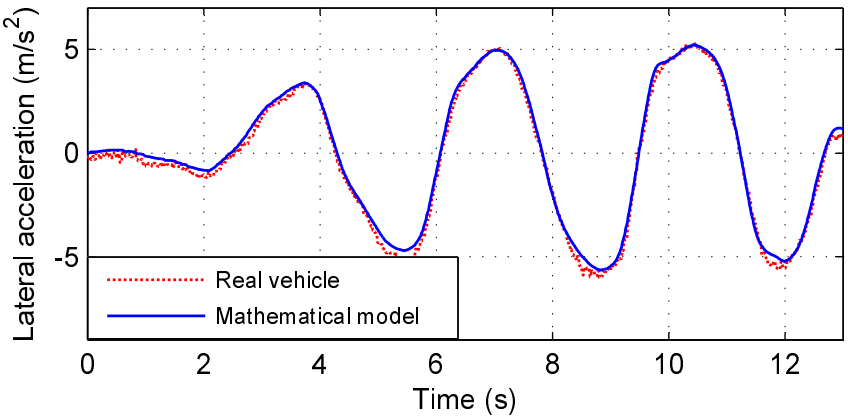

(a) lateral acceleration in slalom maneuver

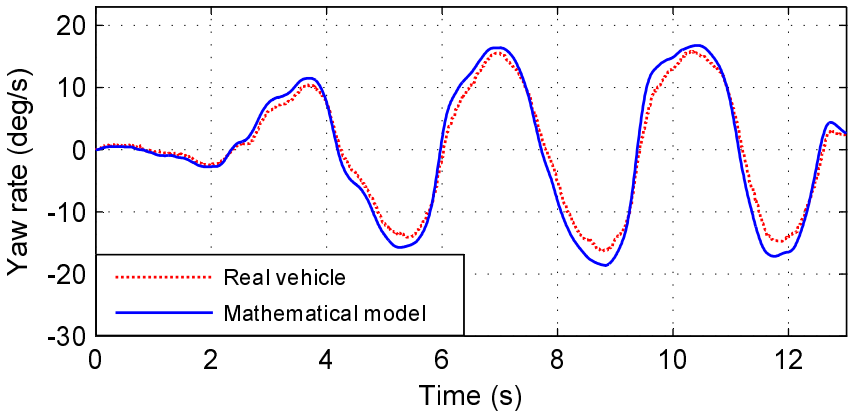

(b) yaw rate in slalom maneuver

Figure 10: Comparison results of slalom maneuver test

model components and external vehicle controllers [36]. Therefore, in this manuscript, veDYNA®-Simulink joint simulations in different running conditions are carried out based on fully automated vehicle model of Hongqi vehicle HQ430, which are built in the framework of veDYNA and about 260 parameters are identified from about 2000 experiment data. The comparisons between HQ430 model and experimental results are carried out to test the precision of the Hongqi vehicle HQ430 model. Due to the large amount of experimental data, here two typical groups of the comparison results are shown in Fig. 9 and Fig. 10, in which Fig. 9 are obtained from one hundred kilometers acceleration test and Fig. 10 are obtained from slalom manoeuver at 65 km/h. From the tests

above, the qualified longitudinal and lateral dynamic precisions of this mathematical model could be obtained.

Based on the high-precision vehicle model, the effective verification and comparisons between the presented method and its original form that is not consider modelling error are carried out. In addition, the parameters of Hongqi vehicle HQ430 used here are shown in Table 1.

Table 1: Parameters of Hongqi vehicle HQ430 and used in the controller design

Symbol	Description	Value	Unit
a	distance from CoG to front axle	1.5	[m]
b	distance from CoG to rear axle	1.35	[m]
I_z	yaw rate of inertia around CoG	3411.52	[kg $\cdot$ m^2]
m	mass of vehicle	2160	[kg]
C_f	cornering stiffness of front axle	-87594	[N/rad]
C_r	cornering stiffness of rear axle	-87594	[N/rad]
ω	vehicle width	1.795	[m]
l_f	CoG to front end	2.5575	[m]
l_r	CoG to rear end	2.4075	[m]
δ_{fsat}	maximum control action	30	[°]
$\Delta\delta_{fsat}$	maximum variance control action	9.5	[°/s]

4.1. Double lane change manoeuver

Various running conditions are carried out to test the effectiveness of the proposed dual-envelop-oriented moving horizon path tracking method. Considering it is easily unstable as vehicles make a sharp turn, double lane change manoeuver is carried out on dry asphalt pavement with tire-road friction coefficient $\mu = 0.9$ and $v = 90$ km/h to verify the effectiveness of the proposed path tracking method. The simulation results are shown in Fig. 11, where the path trajectory of vehicle is shown in Fig. 11 (a), the computational time of the proposed controller is given in Fig. 11 (b), and the yaw rate and sideslip angle could be seen in Fig. 11 (c) and (d), respectively. The dot in Fig. 11 represents the simulation result considering modelling error. The dash dot line expresses

the control performance of varied sample time. The dotted line shown the control performance of varied predictive horizon. The solid line expresses the simulation results of the proposed controller adopted in this paper. In addition, the dash line shows the performance of the original controller without considering modelling error, varied sample and predictive horizon.

It can be seen from Fig. 11 (a) that the controlled vehicle keeps running in the O-ENV, which indicates that the presented dual-envelop-oriented moving horizon path tracking controller performs well on the dry asphalt pavement. Moreover, the lateral tracking error is decreased when the optimization issue in Eq. (30) is described using the improved model in Eq. (21). In addition, the computational time is also decreased as shown in Fig. 11 (b) using the improved model. The tracking error is further decreased and the computational time is further decreased by introducing varied sample time. Moreover, better tracking error and computational time could be obtained using the varied predictive horizon compared with varied sample time which could be seen from Fig. 11 (a) and (b). In addition, the lateral stability described by yaw rate and sideslip angle could also be improved seen from Fig. 11 (c) and (d). It verifies that the proposed controller could make the controlled vehicle run safely and stably. As a result, the simulation results that employ the varied predictive horizon and sample time by the means of the improved vehicle model obtain the most favourite performance compared with the single improvement of the above three situations. It is specified that the proposed moving horizon path tracking method obtains better tracking performance. Moreover, concluded from the above simulation results, the improved model and the varied sample time play an important role in path tracking performance improvement.

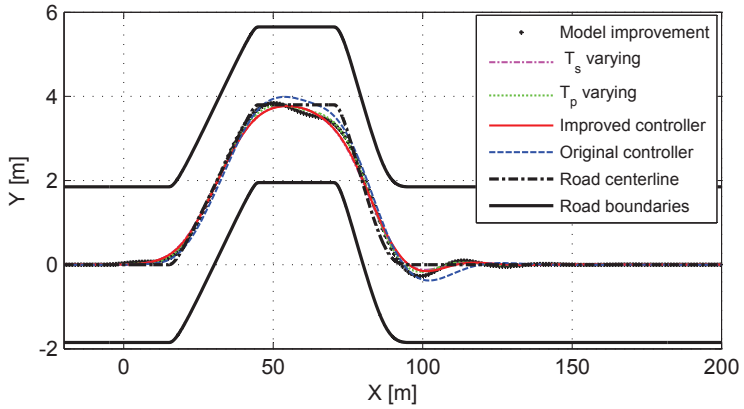

(a) path trajectory of vehicle

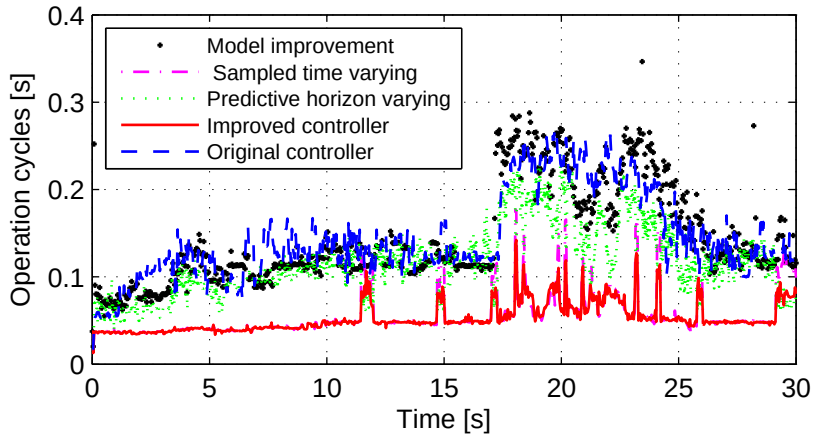

(b) computational time of controller

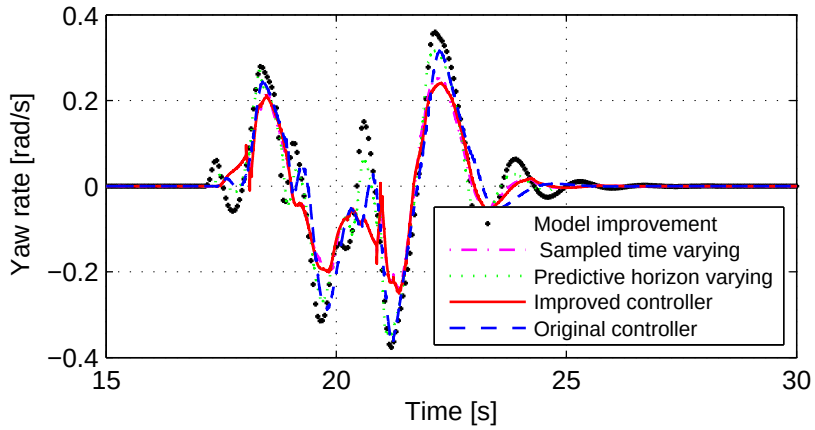

(c) yaw rate r

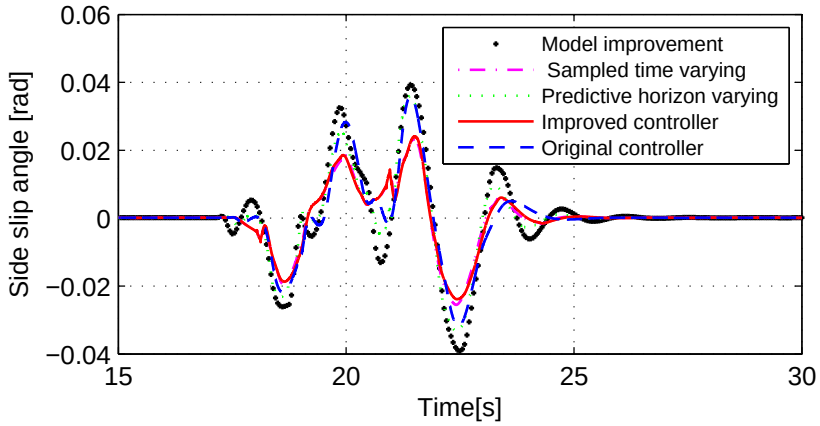

(d) sideslip angle β

Figure 11: Simulation results of double lane change manoeuver

4.2. Slalom maneuver

In order to further verify the effectiveness of the improved dual-envelop-oriented moving horizon path tracking method, slalom maneuver is carried out on the dry asphalt pavement with tire-road friction coefficient $\mu = 0.9$ and $v = 65$ km/h. The simulation results of path trajectory, computational time, yaw rate, and sideslip angle could be seen from Fig. 12 (a) - (d), respectively. The meanings of the lines in Fig. 12 are the same as the above double lane change manoeuver.

In this situation, the vehicle still runs in the O-ENV. The tracking error could be decreased and the computational time is also reduced by considering modelling error and introducing the varied sample time and varied predictive time. It satisfies the requirement of active safety control system

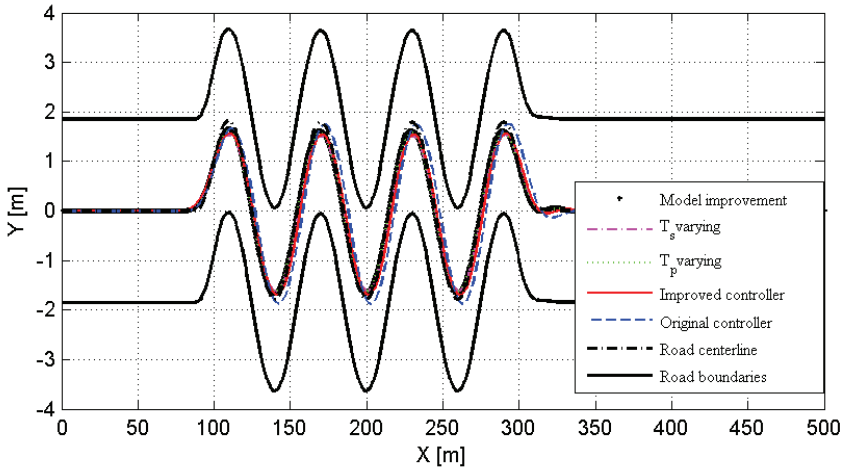

(a) vehicle path trajectory

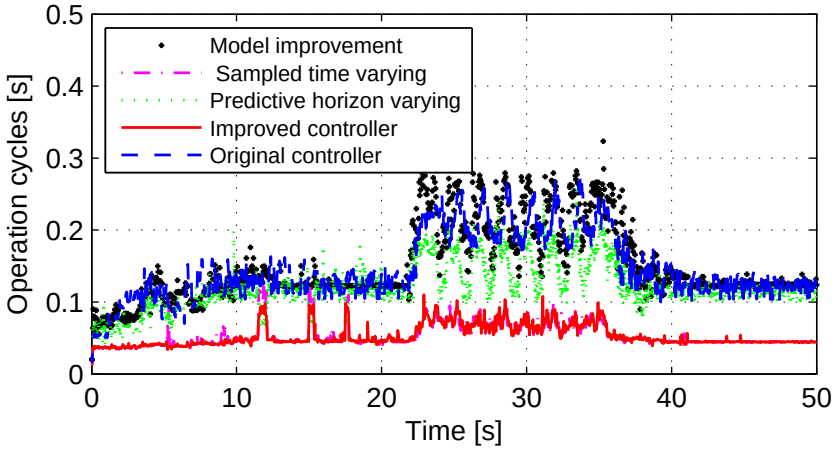

(b) computational time

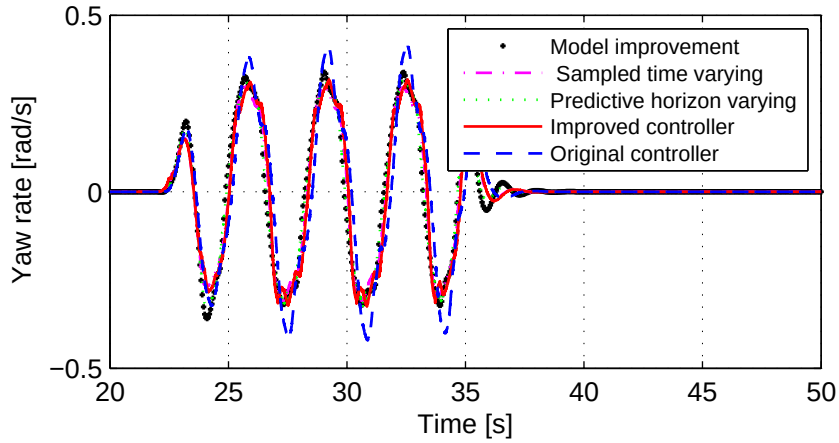

(c) yaw rate r

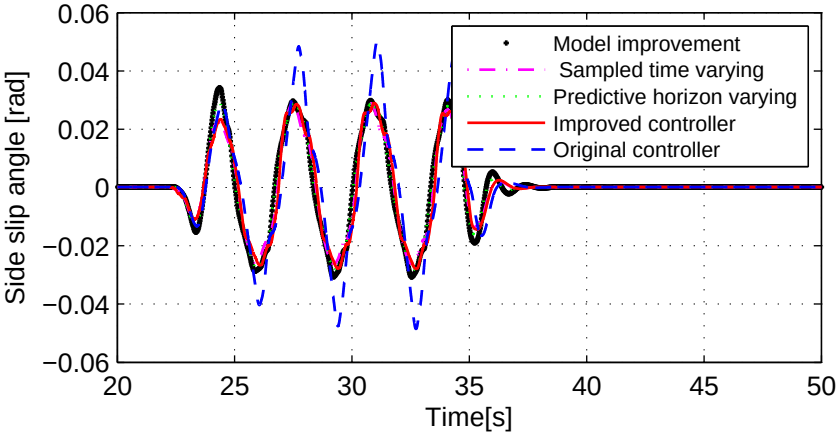

(d) vehicle sideslip angle β

Figure 12: Simulation results of slalom maneuver

seen from Fig. 12 (a) and (b). Moreover, It is shown in Fig. 12 (c) and (d) that the yaw rate and sideslip angle could also be improved to some extent by enhancing the precision of vehicle model. It specifies that the better tracking performance could be obtained using the proposed dual-envelop-oriented moving horizon path tracking method in slalom maneuver condition.

Besides the above simulations, the proposed dual-envelop-oriented moving horizon path tracking method is verified on the slippery road and the similar results could be obtained. Due to space limitation, the veDYNA-Simulink joint simulations are not presented here. Based on these simulation results in different running conditions, the proposed algorithm obtains good path tracking

performance. Besides, it could be seen that the controlled vehicle obtains improved stable performance along with the improved vehicle model, varied sample time, and varied predictive horizon. Therefore, the proposed dual-envelop-oriented moving horizon path tracking method could be applied to various vehicle running conditions.

4.3. Effectiveness validation of inner-envelop and outer-envelop

In order to specify the effectiveness of the dual-envelop, the proposed path moving horizon tracking method is verified without inner-envelop and dual-envelop, respectively. The vehicle runs in the double lane change manoeuver at the speed of $v_x = 88$km/h with tire-road coefficient is $\mu = 0.6$. The comparison results between the proposed dual-envelop-oriented path moving horizon tracking method and the path tracking method that did not consider the inner-envelop and dual-envelop are shown in Fig. 13 (a)-(d), clearly. In Fig. 13 (a) the dotted line represents the path moving horizon tracking method that did not consider the inner-envelop, the dash dotted line stands for the presented method that did not consider the dual-envelop, and the solid line represent the proposed method in this manuscript that both consider the inner-envelop and outer-envelop. The lines in Fig. 13 (b) and (c) contains the same implications.

It can be seen from Fig. 13 (a) that the controlled vehicle keeps running in the O-ENV when the I-ENV is not consider as constraints. However, the tracking precision is worse than the proposed method that taken the I-ENV as constraints. Besides, the front steering angle shown in Fig. 13 (b) is larger when the relative big tracking error obtained. It is specified that it is effective considering the I-ENV in the proposed path moving horizon tracking method. When the dual-envelop both are not considered as constraints in the presented method, the vehicle can not track the desired road and the trajectory went beyond the road boundary constraints that can be seen in Fig. 13 (a), clearly. Moreover, the vehicle can not keep stable in this situation that could be seen in Fig. 13 (c)-(d), respectively. It indicates that it obtains actual benefit when considers the dual-envelop as constraints in the proposed controller in this running condition. Therefore, it is necessary to consider the I-ENV and O-ENV in the presented method, and is actually important to consider the dual-envelop to path tracking issues.

Besides the situation discussed above, it can be seen from Fig. 13 (d) that the sideslip angle

sometimes reaches a peak value of about 6° in dual-envelop considered situation. Compared to the situation that did not consider the I-ENV, the boundaries is not reduced by half width of vehicle. The vehicle running region is relatively larger than dual-envelop considered situation. Therefore, sideslip angle is smaller than the dual-envelop considered situation. In addition, from the respective of optimization, the reason maybe that in the optimization function, the main objective is to make the vehicle follow the road centerline and keep the vehicle in the O-ENV. The vehicle states, for example sideslip angle and yaw rate did not considered here. In order to obtain the optimized value of front steering angle to follow the road centerline line, sometimes the performance of sideslip angle is affected. Therefore, it is necessary to consider the constraints of sideslip angle in controller formulation and it will discussed in details in our further work.

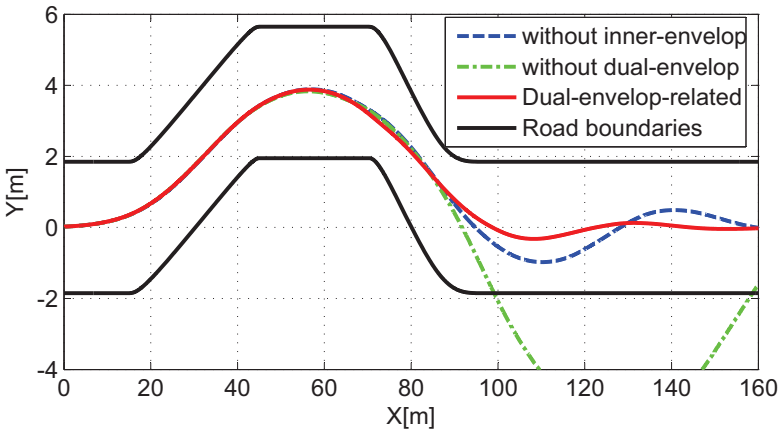

(a) vehicle path trajectory

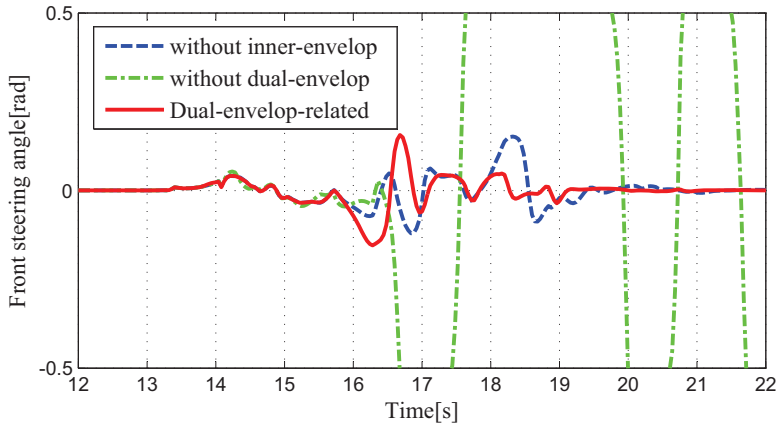

(b) front steering angle

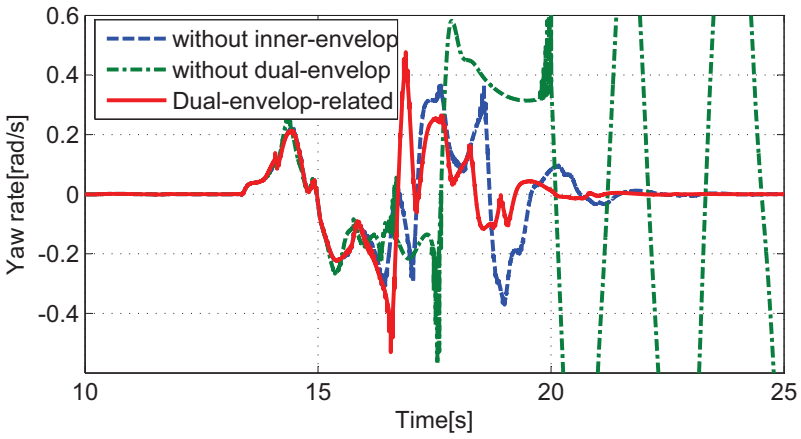

(c) yaw rate r

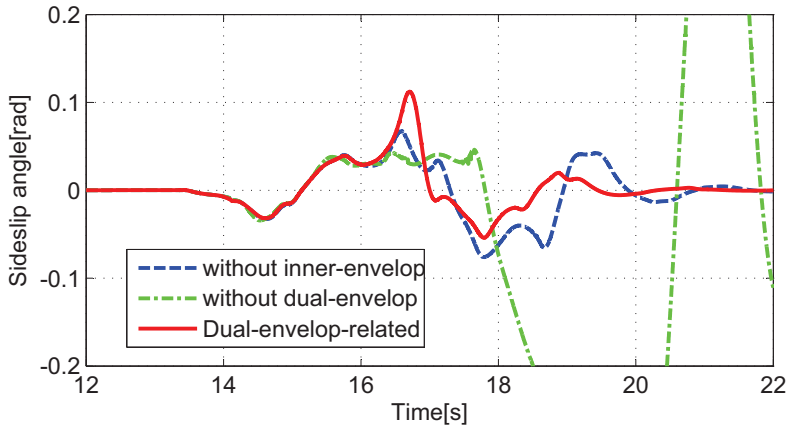

(d) vehicle sideslip angle β

Figure 13: Effectiveness of inner-envelop and outer envelop

4.4. Tire-road friction coefficient varied situation

In order to validate the reaction of the proposed dual-envelop-oriented path tracking controller on quick variation of the tire-road friction coefficient when vehicle is cornering, double lane change manoeuver simulations are carried out. In this situation, vehicle is accelerated from stationary to speed $v_x = 60$ and the tire-road friction is $\mu = 0.6$ at the beginning of the acceleration. When the vehicle first change lane, the tire-road friction coefficient is change to $\mu = 0.4$ and the vehicle keep speed invariant. Then the tire-road friction coefficient is changed to the original value $\mu = 0.6$ at the rest road. The path trajectory, front steering angle, yaw rate and sideslip angle in this situation are shown in Fig. 14 (a)-(d), respectively.

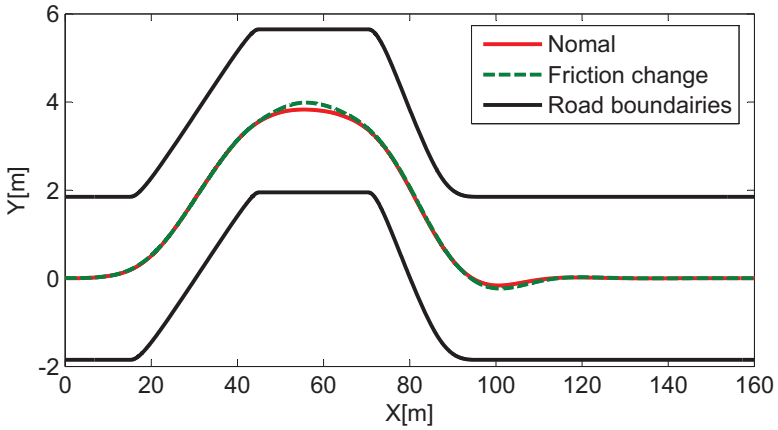

(a) vehicle path trajectory

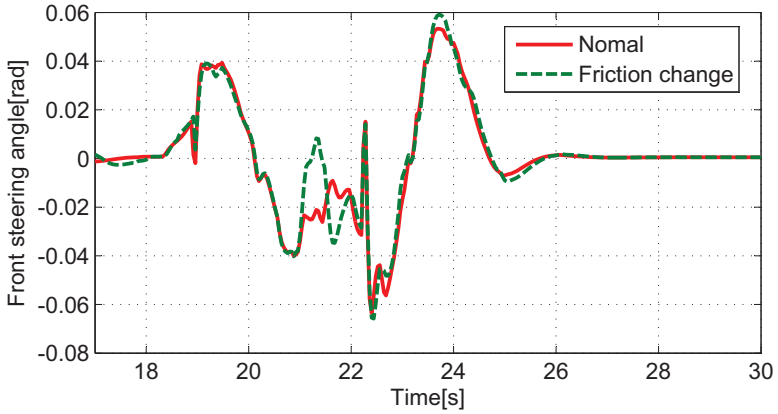

(b) front steering angle

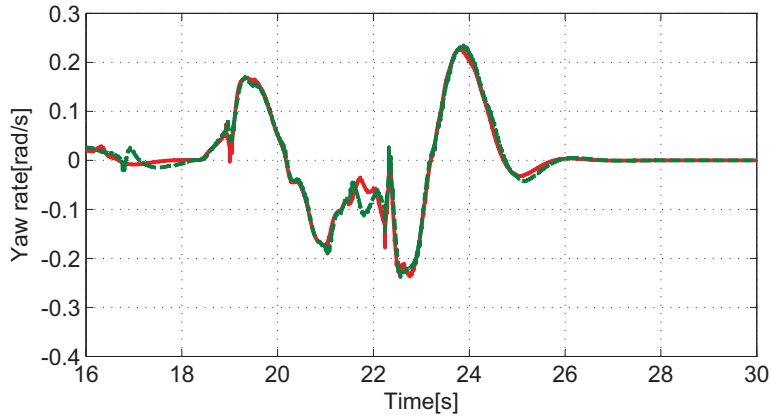

(c) yaw rate r

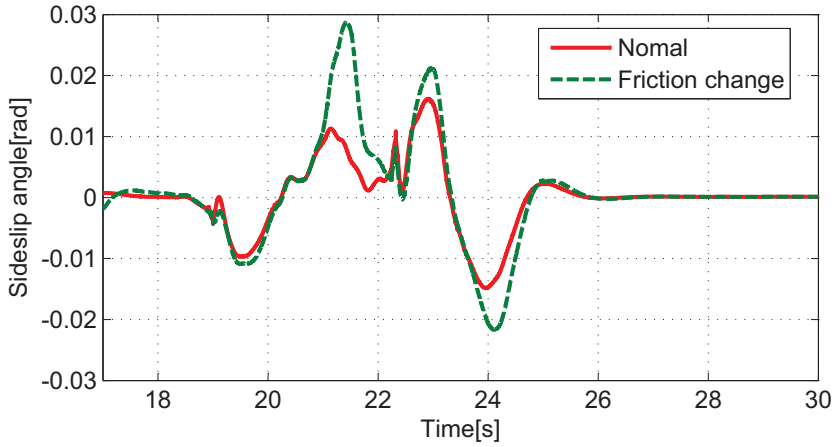

(d) vehicle sideslip angle β

Figure 14: Simulation results of varied tire-road friction coefficient

It can be seen from Fig. 14 (a) that the proposed method could finish the double lane change manoeuver within road boundaries when tire-road friction coefficient quick varied. Compared with the tire-road friction coefficient keep invariant situation, the trajectory only has a small difference. The optimized front steering angle shown in Fig. 14 (b) is regulated by the controller accordingly when the tire-road friction coefficient is varied. It also makes small variation of yaw rate and sideslip angle that shown in Fig. 14 (c) and (d), respectively. Considering from the respective of vehicle dynamics, the vehicle dynamic state is changed when the control input that is front steering angle varied. From the above simulation results, it is specified that the proposed dual-envelop-oriented path moving horizon tracking scheme could finish the double lane change manoeuver mentioned above facing quick variations of tire-road friction coefficient. It could also concluded that the proposed path tracking controller is robust facing quick variation of tire-road coefficient in this situation.

5. CONCLUSION

Dual-envelop-oriented moving horizon path tracking issue for fully automated vehicles is described uniquely in this manuscript, in which the shape of vehicle is considered as inner-envelop (I-ENV) and the feasible road region is described as outer-envelop (O-ENV). Then the moving

horizon path tracking method is proposed employing model predictive control (MPC) method, in which the front wheel steering angle is selected as the control variable, and the actuator constraints are also considered. Moreover, the proposed dual-envelop-oriented path tracking method is discussed from the aspects of modelling error, varied sample time, and varied predictive time. The proposed dual-envelop-oriented moving horizon path tracking method is verified effective in double lane change manoeuver, slalom manoeuver, and tire-road friction coefficient varied, etc running condition and keep fully automated vehicle run safely and stably. Moreover, the presented path tracking method could obtain better tracking precision.

For further research, the varied constraints of maximum and minimum front steering wheel angle will be considered. In addition, the heading angle error should be discussed in details, and the constraints of vehicle states such as yaw rate, yaw angle and sideslip angle should be considered.

ACKNOWLEDGMENT

This work is supported by the National Nature Science Foundation of China (91220301, 61403158, 61573165), the Project of the Education Department of Jilin Province (2016-429), the Open Fund Project of the State Key Laboratory of Automotive Simulation and Control in Jilin University.

References

[1] S. B. Li,H. Peng, Strategies to minimize the fuel consumption of passenger cars during car-following scenarios, Proceedings of the Institution of Mechanical Engineers, Part D: Journal of Automobile Engineering 226 (3) (2012) 419–429.

[2] S. B. Li, K. Q. Li, J. Q. Wang, Economy-oriented vehicle adaptive cruise control with coordinating multiple objectives function, Vehicle System Dynamics: International Journal of Vehicle Mechanics and Mobility 51 (1) (2013) 1–17.

[3] L. D. Novellis, A. Sorniotti, P. Gruber, J. Orus, J. M. R. Fortun, J. Theunissen, J. D. Smet, Direct yaw moment control actuated through electric drivetrains and friction brakes: Theoretical design and experimental assessment, Mechatronics 26 (1) (2015) 1–15.

[4] J. Yoon, W. Cho, B. Koo, K. Yi, Unified chassis control for rollover prevention and lateral stability, IEEE Transaction on Vehicular Technology 58 (2) (2009) 596–609.

[5] F. Wang, H. Chen, H. Y. Guo, D. P. Cao, Constraint H_∞ control for road vehicles after a tire blow-out, Mechatronics 30 (5) (2015) 371–382.

[6] D. González, J. Pérez, V. Milanéz, F. Nashashibi, A review of motion planning techniques for automomated vehicles, IEEE Transaction on Intllignet Transportation Systmes 17 (4) (2016) 1135–1145.

[7] M. Brown, J. Funke, S. Erlien, J. C. Gerdes, Safe driving envelopes for path tracking in autonomous vehicles, Control Engineering Practice (2016) In Press.

[8] T. Shim, G. Adireddy, H. Yuan, Autonomous vehicle collision avoidance system using path planning and model-predictive-control-based active front steering and wheel torque control, Journal of Automobile Engineering-Part D 226 (6) (2012) 767–778.

[9] Y. Chen, J. Wang, Adaptive vehicle speed control with input injections for longitudinal motion independent toad frictional condition estimation, IEEE Transactions on Vehicular Technology 60 (3) (2011) 839–848.

[10] J. Wang, Q. Wang, L. Jin, C. Song, Independent wheel torque control of 4WD electric vehicle for differential drive assisted steering, Mechatronics 21 (1) (2011) 63–76.

[11] L. Lapierre, B. Jouvencel, Robust nonlinear path-following control of an AUV, IEEE Journal of Oceanic Engineering 33 (2) (2008) 89–102.

[12] Q. Zhang, D. Wu, J. F. Reid, E. R. Benson, Model recogintion and validation for an off-road vehicle electrohydraulic steering controller, Mechatronics 12 (6) (2002) 845–858.

[13] B. Bayar, M. Bergerman, E. I. Konukseven, A. B. Koku, Improving the tracjectory tracking performance of autonomous archard vehicles using wheel slip compensation, Biosystmes Engineering (2016) In Press.

[14] V. Girbés, L. Armesto, J. Torenro, Path following hybrid control for vehicle stability applied to industrial forklifts, Robotics & Autonomous Systmes 62 (6) (2014) 910–922.

[15] E. Maalout, M. Saad, H. Saliah, A higher level path tracking controller for a four-wheel differentially steered mobile robot, Robotics and Autonomous Systems 54 (1) (2006) 23–33.

[16] C. Hu, H. Jing, R. Wang, F. Yan, M. Chadli, Robust H_∞ output-feedback control for path following of autonomous ground vehicles, Mechanical Systems and Signal Processing 70-71 (2015) 414–427.

[17] C. Hu, R. Wang, F. Yan, N. Chen, Output constraint control on path following of four-wheel independently actuated autonomous vehicles, IEEE Transactions on Vehicular Technology In Press.

[18] R. Wang, C. Hu, F. Yan, M. Chadli, Composite nonlinear feedback control for path following of four-wheel independently actuated autonomous ground vehicles, IEEE Transactions on Intelligent Transportation Systems (2016) In press.

[19] C. Hu, R. Wang, F. Yan, Integral sliding mode-based composite nonlinear feedback control for path following of four-wheel independently actuated autonomous vehicles, IEEE Transactions on Transportation Electrification 2(2) (2016) 221-230.

[20] Y. Wang, S. P. Boyd, Fast model predictive control using online optimization, IEEE Transactions on Control Systems Technology 41 (2) (2008) 6974–6979.

[21] H. Chen, F. Xu, Y. Xi, Field programmable gate array/system on a programmable chip based implementation of model predictive controller, IET Control Theory & Applications 6 (8) (2012) 1055–1063.

[22] S. B. Li, K. Q. Li, R. Rajamani, J. Q. Wang, Model predictive multi-objective vehicular adaptive cruise control, IEEE Transactions on Control Systems Technology 19 (3) (2011) 556–566.

[23] S. B. Li, S. B. Xu, D. Kum, Efficient and accurate computation of model predictive control using pseudospectral discretization, Neurocomputing 177 (2016) 363–372.

[24] R. Schmied, H. Waschl, R. Quirynen, M. Diehl, D. R. L., Nonlinear MPC for emission efficient cooperative adaptive cruise control, in: IFAC Conference on Nonlinear Model Predictive Control, IFAC Paperonline, Seville, Spain, 2015, pp. 160–165.

[25] H. Zhang, J. Wang, Vehicle lateral dynamics control through AFS/DYC and robust gain-scheduling approach, IEEE Transactions on Vehicular Technology 65 (1) (2016) 489–494.

[26] S. J. Qin, A. Thomas, A. Badgwell, A survey of industrial model predictive control technology, Control Engineering Practice 11 (2003) 733–764.

[27] G. V. Raffo, G. K. Gomes, J. E. Normey-Rico, C. R. Kelber, L. B. Becker, A predictive controller for autonomous vehicle path tracking, IEEE Transactions on Intelligent Transportation Systems 10 (1) (2009) 92–102.

[28] F. Borrelli, P. Keviczky, T. Asgari, D. Hrovat, MPC-based approach to active steering for autonomous vehicle systems, International Journal of Vehicle Autonomous Systems 3 (2) (2005) 265–291.

[29] H. Dahmani, M. Chadli, A. Rabhi, A. Hajjaji, Road curvature estimation for vehicle lane departure detection using a robust takagi-sugeno fuzzy observer, Vehicle Systme Dynamics 51 (5) (2013) 581–599.

[30] R. Yu, H. Guo, Z. Sun, H. Chen, MPC-based regional path tracking controller design for autonomous ground vehicles, in: Proceedings of 2015 IEEE International Conference on Systems, Man, and Cybernetics, IEEE, Hongkong, 2015, pp. 2510–2515.

[31] H. Y. Guo, F. Liu, R. Yu, Z.P. Sun, H. Chen, Regional path moving horizon tracking controller design for autonomous ground vehicles. Science China Information Science, 2017, 60(1): online.

[32] J. Wang, L. Alexander, R. Rajamani, Friction estimation on highway vehicles using longitudinal measurements, Journal of Dynamic Systems, Measurement, and Control 126 (2) (2004) 265–275.

[33] R. Rajamani, G. Phanomchoeng, D. Piyabongkarn, J. Y. Lew, Algorithms for real-time estimation of individual wheel tire-road friction coefficients, IEEE/ASME Transactions on Mechatornics 17 (6) (2012) 1183–1195.

[34] B. Y. Li, H. P. Du, W. H. Li, Y. J. Zhang, Side-slip angle estimation based lateral dynamics control for omni-directional vehicles with optimal steering angle and traction/brake torque distribution, Mechatronics 30 (5) (2015) 348–362.

[35] B. C. Chen, C. T. Tsai, and K. Lee, October 9-12, 2015, Path-following steering controller of automated lane change system with adaptive preview time, in Proceedings of 2015 IEEE International Conference on Systems, Man, and Cybernetics, IEEE, Hong Kong, 2015, pp: 2522-2526.

[36] H. Y. Guo, H. Chen, D. P. Cao, and W. W. Jin, Design of a reduced-order non-linear observer for vehicle velocities estimation, IET Control Theory and Applications 17 (7) (2013) 2056–2068.

Cranfield University

CERES https://dspace.lib.cranfield.ac.uk

School of Aerospace, Transport and Manufacturing (SATM) Staff publications (SATM)

2017-02-14

Dual-envelop-oriented moving horizon path tracking control for fully automated vehicles

Guo, Hongyan

Elsevier

Hongyan Guo, Jun Liu, Dongpu Cao, Hong Chen, Ru Yu, Chen Lv, Dual-envelop-oriented moving horizon path tracking control for fully automated vehicles, Mechatronics, Vol. 50, April 2018, pp. 422-433

https://dspace.lib.cranfield.ac.uk/handle/1826/11845

Downloaded from Cranfield Library Services E-Repository